Shape changes and alignment properties in ^{77}Kr

C. J. Gross, P. D. Cottle, D. M. Headly,* U. J. Hüttmeier,
E. F. Moore, and S. L. Tabor
Department of Physics, Florida State University, Tallahassee, Florida 32306

W. Nazarewicz†
Supercomputer Computations Research Institute, Florida State University, Tallahassee, Florida 32306
and The Niels Bohr Institute, DK-2100 Copenhagen Ø, Denmark
(Received 30 June 1987)

Excited positive parity states up to spin $(\frac{41}{2})$ have been studied in ^{77}Kr using a 98 MeV ^{28}Si beam on a natural chromium target. $\Delta J=1$ transitions have been identified throughout the positive parity band. The energies, mixing ratios, and $B(M1)$ transition rates for these transitions alternate in size as the spin increases. A cranked shell model analysis was performed along with Strutinsky-Bogolyubov cranking calculations. The observed decrease in the signature splitting of the $\nu g_{9/2}$ band has been attributed to a band crossing due to an aligning pair of $g_{9/2}$ protons. Prolate quadrupole deformations of $\beta_2=0.34$ for the one-quasiparticle band and $\beta_2=0.26$ for the three-quasiparticle band are predicted. This band crossing is associated with a shape change caused by the polarization effect of aligned quasiparticles.

I. INTRODUCTION

The neutron deficient bromine, krypton, and strontium isotopes offer some of the best examples of large collective quadrupole deformations and shape coexistence. The nuclei ^{76}Kr and ^{78}Kr, in particular, are predicted to have strong prolate deformations coexisting with oblate structures. These competing deformations produce nuclei that are γ soft, especially at low angular momenta. However, these nuclei behave collectively at high spins. These phenomena can be fairly well described by the deformed shell model.

Previously, ^{77}Kr has been studied in detail[1,2] up to the $J^{\pi}=\frac{25}{2}^{+}$, 4153 keV level using ^{16}O beams. The one-quasiparticle (1qp) neutron states have been studied up to the onset of the three-quasiparticle (3qp) excitations. The present work was initiated to extend our knowledge beyond the 3qp excitations by using a heavier beam (^{28}Si) to excite higher spin states.

Two different targets, ^{52}Cr and ^{55}Mn, were used to study ^{77}Kr. The ^{55}Mn(^{28}Si,αpn)^{77}Kr reaction at 108 MeV and the ^{52}Cr(^{28}Si,2pn)^{77}Kr reaction at 98 MeV produce a moderate percentage of ^{77}Kr out of all the fusion-evaporation products; however, the 2pn channel populated more higher spin states cleanly. Thus, the data contained in this report was taken using the chromium reaction.

II. EXPERIMENTAL PROCEDURE

High spin states in ^{77}Kr were observed using the reaction ^{52}Cr(^{28}Si,2pn)^{77}Kr at 98 MeV. The ^{28}Si beam was produced using the Florida State University FN tandem accelerator. The beam was stripped to a charge of 8^{+} at the terminal and stripped again midway down the high energy column to a charge of 12^{+}. The chromium target was made of natural chromium, which contains approximately 84% ^{52}Cr. About 1 mg/cm^2 of chromium was evaporated on an 0.013 cm thick lead foil.

The γ rays were detected with two Compton-suppressed intrinsic germanium detectors, each with an efficiency of about 24%. A ^{152}Eu source was used to determine relative efficiencies and the energy calibrations of the detectors. The energy resolution of the 1333 keV transition in ^{60}Co was better than 2.5 keV.

γ-γ coincidence data were taken with a detector on both sides of the beam line at 81° in the forward direction. This detector arrangement was used to reduce the 511 keV annihilation coincidences and still minimize the Doppler shift which occurs at angles other than 90°.

All data were stored on magnetic tape for later analysis. Three parameters were stored for each coincidence event, two energy events and a time-to-amplitude converter (TAC), which represented the time difference between the two detectors. The TAC was gated, and the subsequent energy parameters were sorted on a 2500×2500 two-dimensional array using a μ-VAXII computer. One-dimensional energy spectra were then projected out of the array corresponding to particular energy gates and equal sized Compton background subtract gates.

Angular distribution data were taken with one detector positioned at 90° with respect to the beam axis to serve as a normalization check. On the other side of the beam axis, a movable detector was placed at 90°, 60°, 45°, 30°, and 0°.

III. EXPERIMENTAL RESULTS

The level scheme for the yrast positive parity band in ^{77}Kr based on the present work is shown in Fig. 1. The present study confirms the positive parity levels up to

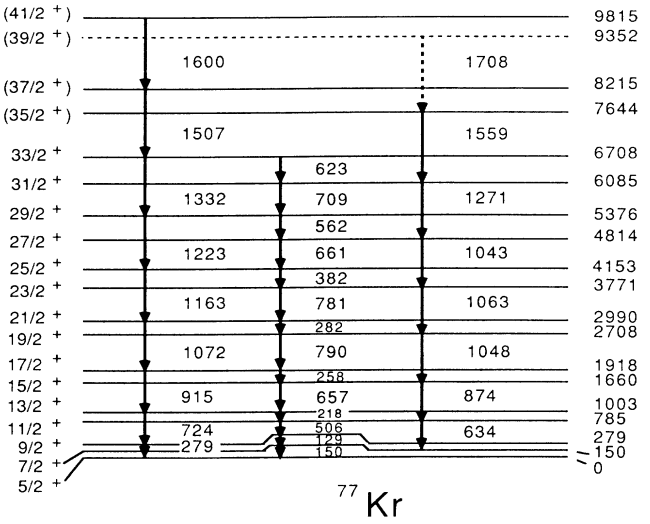

FIG. 1. Proposed level scheme of yrast band in ^{77}Kr as deduced from the present work and previous studies. Transitions in the $\alpha=+\frac{1}{2}$ band are to the left and those in the $\alpha=-\frac{1}{2}$ band are to the right.

4153 keV, $\frac{25}{2}^+$, and negative parity levels up to 3605 keV, $\frac{21}{2}^-$, that have been reported in Refs. 1 and 2. In addition, we have extended the positive parity yrast sequence up to a state of $J^\pi=(\frac{41}{2}^+)$ as shown in Fig. 1.

Figure 2 shows the sum of the coincidence spectra gated on the 129 + 150 + 724 + 915 keV transitions.

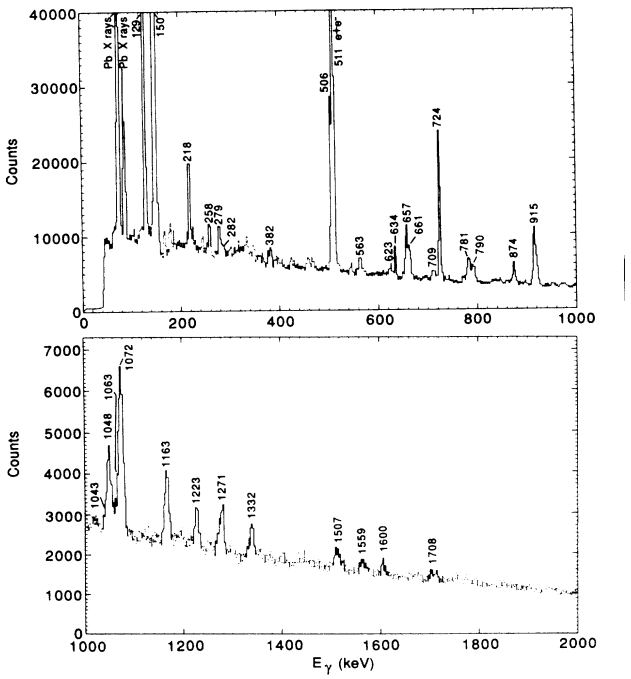

FIG. 2. Coincidence spectra generated by the addition of several gates—the 129, 150, 724, and 915 keV gates. All transitions lie in ^{77}Kr unless otherwise indicated. The 150 keV line has some 147 keV contaminant due to the 130 keV transition in ^{77}Br. Some peaks may be Doppler shifted with a $\beta\simeq 0.017$.

All the high spin transitions seen previously can be observed. Although transitions coming from $\frac{25}{2}^+$ state were seen before, the transitions decaying to the $\frac{19}{2}^+$ state had been only tentatively identified. These transitions, the 282 and 1063 keV peaks, are shown in Figs. 3 and 4(a), respectively.

As seen in the level scheme, several transitions have similar energies. The 282 keV $\frac{21}{2}^+\rightarrow\frac{19}{2}^+$ transition can be observed in Fig. 3. The 150 keV gated spectrum does not have the 279 keV transition which masks the much weaker 282 keV line in most of the other gated spectra.

Although the energy differences of the transitions between 1000 and 1100 keV are much greater than the detector resolution, Doppler broadening due to their short lifetimes has made identification of these transitions difficult. A clear identification of the 1063 keV transition is seen in Fig. 4(a). The 1048 keV gate does not have the 1072 keV peak which obscures the 1063 keV transition. Similarly, the 1072 keV gated spectrum shown in Fig. 4(b), allows the identification of the much weaker 1043 keV line.

This same region of the level scheme shows the diminishing of the signature splitting that is characteristic at lower spins (see Sec. V A). The intensities of the $\Delta J=2$ transitions of the unfavored signature band, $\alpha=-\frac{1}{2}$, increase above the 1043 keV transition as compared to those below this transition. In comparing the $\Delta J=1$ transitions above and below the 4153 keV level, the $\alpha=+\frac{1}{2}\rightarrow-\frac{1}{2}$ (type *A*) branching ratios increase. The $\alpha=-\frac{1}{2}\rightarrow+\frac{1}{2}$ (type *B*) transitions remain moderately intense. The presence of all the $\Delta J=1$ transitions provides solid evidence for the placement of the $\Delta J=2$ transitions.

Figure 5 shows a region taken from several gated spectra superimposed on each other to aid the reader in determining the placement of the $\Delta J=2$ transitions in the vicinity of the band crossing. The spectrum in Fig. 5(a) is gated by the 1163 keV transition and shows the 1223, 1271, and 1332 keV transitions. The 1223 keV gated spectrum in Fig. 5(b) shows that the 1271 keV transition is not visible above the background. In Fig.

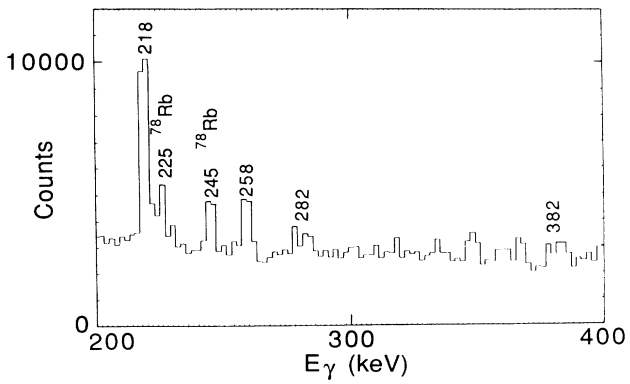

FIG. 3. Partial coincidence spectrum from the 150 keV gate highlighting the 282 keV transition. Unless otherwise indicated, all peaks are in ^{77}Kr. Some peaks may be Doppler shifted with a $\beta\simeq 0.017$.

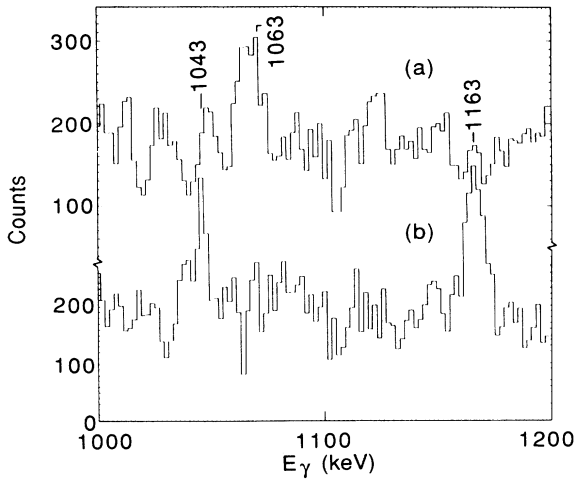

FIG. 4. Partial coincidence spectra highlighting the 1043 and 1063 keV transitions. (a) is the 1048 keV gate clearly showing the 1063 keV transition. The 1043 keV line is also seen. (b) is the 1072 keV gate showing the 1043 keV transition. The 1163 keV line is also seen.

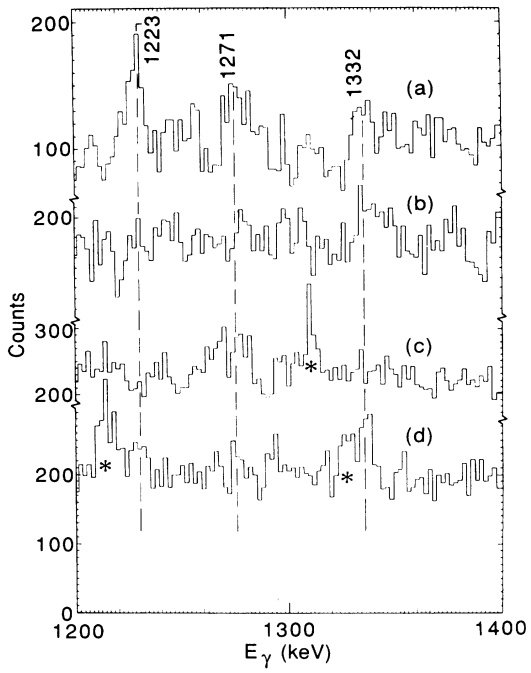

FIG. 5. Partial coincidence spectra from several gates highlighting the transitions in the yrast part of the 3qp band. * indicates contaminants and are explained in the text. (a) is the 1163 keV gate showing the three peaks of interest. (b) is the 1223 keV gate showing only the 1332 keV line. (c) is the 661 keV gate showing only the 1271 keV transition. (d) is the 562 keV gate showing only the 1332 keV line. These peaks are Doppler shifted with a $\beta \simeq 0.017$.

5(c), which illustrates the spectrum in coincidence with the 661 keV γ ray, the 1271 keV line is present. Contaminant lines from ^{78}Kr are due to gating on the 664 keV $4^+ \rightarrow 2^+$ transition.[3] The 562 keV gated spectrum in Fig. 5(d) shows neither the 1223 nor 1271 keV transitions but does show the 1332 keV peak. Contaminant lines from ^{75}Br are from the 563 keV $\frac{13}{2}^+ \rightarrow \frac{9}{2}^+$ transition.[4] This evidence, plus the visible $\Delta J = 1$ transitions, establishes this section of the level scheme shown in Fig. 1.

Above the 7644 keV level we see the strengthening of the signature splitting again. The $\Delta J = 1$ transitions are not seen and therefore we have labeled the 9352 keV level as tentative.

Table I contains the γ-ray transition energies, their relative intensities as compared to the strength of the 724 keV transition, and a comparison between branching ratios from the past and present work. Uncertainties in the relative intensities are estimated to be about $\pm 10\%$.

Branching ratios from Ref. 1 were derived from the relative intensities of the γ rays at 55°. The present intensities and branching ratios were derived from the coincidence data taken at 81°, using the yields of the 150 and 279 keV gates added together to allow for all possible decay paths. This procedure helps to eliminate interference from other nuclei demonstrated by the large yields of contaminants in Figs. 5(c) and 5(d).

One problem with this technique is that angular correlations can substantially affect the yields generated. In order to partially correct for this effect the yields have been adjusted by taking into account the ratio of angular distribution results for 81° and 55° for both the particular γ ray and the gate. In cases where the angular distribution was not measured for a $\Delta J = 2$ transition, we used theoretical angular distribution coefficients for a pure quadrupole transition. If the $\Delta J = 1$ angular distributions were not known, the intensities were not corrected. For two levels, 1003 and 1918 keV, angular distributions were measured for both branches and the A_0 coefficients were also used to calculate branching ratios in order to compare results, and these branching ratios are also indicated in Table I.

Table II contains angular distribution coefficients fitted with the Legendre polynomial series

$$Y(\theta) = A_0 * [1 + a_2 * P_2(\cos\theta) + a_4 * P_4(\cos\theta)] \ . \quad (1)$$

The resulting a_2 coefficients are consistent with the spin assignments shown in Fig. 1 up through the level at 5376 keV. The spins of 6085 and 6708 keV levels are based on their decay mode.

The angular distributions were also fitted as a function of δ, the mixing ratio, for particular initial and final spins according to the properties of angular momentum algebra, assuming a Gaussian distribution of substates.[5] A Gaussian width of 2 was assumed as reasonable,[6] although the dependence of the fit on this parameter was small. Figure 6 shows four examples of the normalized χ^2 per degree of freedom[6] versus arctanδ. Figure 6(a) is typical of the fits for the type A transitions; these transitions are almost pure $M1$ in character. Figures 6(b)–6(d) are fits for type B transitions; the transitions shown in Figs. 6(b) and 6(c) have appreciable $E2$ strength. There are two distinct minima, and, as seen in Fig. 6(c), there is some ambiguity about the choice of δ. For all $\Delta J = 1$

TABLE I. Intensities and branching ratios for Ref. 1 and present work.

E level (keV)	E_γ (keV)	I_γ	Branching ratios Ref. 1	Branching ratios Present	Ang dis.[a]
150	150				
279	129				
	279				
785	506	42	72 (3)	75 (3)	
	634	14	28 (3)	25 (3)	
1003	218	22	6 (3)	18 (2)	12 (1)
	724	100	94 (3)	82 (2)	88 (1)
1660	657	26	37 (5)	48 (4)	
	874	28	63 (5)	52 (4)	
1918	258	4	2 (1)	4 (1)	4 (1)
	915	88	98 (1)	96 (1)	96 (1)
2708	790	14		37 (3)	
	1048	24		63 (3)	
2990	282	6[b]	<6	<9[b]	
	1072	59[b]	>94	>91[b]	
3771	781	19		61 (3)	
	1063	12		39 (3)	
4153	382	6	<35	16 (2)	
	1163	31	>65	84 (2)	
4814	661	14		67 (3)[d]	
	1043	7[c]		33 (3)[d]	
5376	562	7		37 (3)	
	1223	12		63 (3)	
6085	709	19[b]		<37[b]	
	1271	16[b]		>63[b]	
6708	623	12[b]		<50[b]	
	1332	11[b]		>50[b]	
7644	1559	8[b]			
8215	1507	16[b]			
9352	1708	6[b]			
9815	1600	8[b]			

[a]Values calculated from the angular distribution A_0 values.
[b]Values were not corrected for angular distribution effects.
[c]Estimated yield due to interference from 1048 keV transition.
[d]Calculated with estimated yield. See footnote c .

transitions except the 790 keV, the only χ^2 minimum which falls below the 0.1% confidence limit has a small positive value of δ. For systematic reasons the small value of δ corresponding to the less favored minimum was listed in Table II for the 790 keV transition. For the two cases that can be compared with Ref. 1, the present values of δ are considerably smaller. We do not know the source of this discrepancy, although the values of δ at the less favored minimum in the present work would better agree with Ref. 1.

IV. DISCUSSION

With the present branching and mixing ratios, we can calculate transition rates using the lifetimes found in Ref. 1. The results are shown in Table III. For the $\Delta J=2$ transitions, there are strong $B(E2)$ values as expected for a collective rotational band. In the $\alpha=+\frac{1}{2}$ band there is a decrease in the $B(E2)$ values between the 1072 and 1163 keV transitions. The reduction in $B(E2)$ strength might be associated with the mixing of the 1qp

TABLE II. Comparison of angular distribution results between previous and present work.

E level (keV)	E_γ (keV)	Ref. 2 A_2/A_0	Ref. 2 A_4/A_0	Ref. 1 A_2/A_0	Ref. 1 A_4/A_0	Ref. 1 $\lvert\delta\rvert$	Present work A_2/A_0	Present work A_4/A_0	Present work $\lvert\delta\rvert$
150	150	−0.36(4)	0.00(4)				a		
279	129	−0.27(32)	0.03(44)				a		
	279	0.29(6)	0.00(9)				0.31(3)	−0.08(3)	
785	506	−0.66(10)	0.01(12)	−0.74(6)	0.07(2)	1.15(15)	−0.63(3)	0.03(3)	0.35(6)
	634						a		
1003	218						−0.29(3)	0.01(3)	0.03(5)
	724	0.32(6)	−0.05(7)	0.29(3)	−0.09(3)		0.30(3)	0.01(3)	
1660	657	−0.50(6)	−0.13(25)	−0.46(7)	0.04(2)	1.5(3)	−0.59(3)	0.06(3)	0.21(5)
	874						a		
1918	258						−0.42(4)	0.05(5)	0.09(7)
	915	0.09(11)	−0.08(14)	0.32(3)	−0.14(3)		0.22(1)	−0.05(3)	
2708	790						−0.83(4)	0.18(5)	0.32(6)
	1048						a		
2990	282						a		
	1072						0.39(3)	−0.06(3)	
3771	781						−0.71(3)	0.06(4)	0.25(6)
	1063						a		
4153	382						−0.35(4)	−0.04(5)	0.07(7)
	1163						a		
4814	661						−0.47(4)	0.08(4)	0.09(5)
5376	562						−0.27(4)	0.03(4)	0.00(7)

[a]Could not be determined.

and 3qp bands (see Sec. V A). The situation in the $\alpha=-\frac{1}{2}$ band is unclear because of the limited lifetime data. The $B(E2)$ values for the $\Delta J=1$ transitions are substantially lower than those reported in Ref. 1 due to the significantly smaller mixing ratios in the present work. The strength of these transitions is constant throughout the reported range within their larger uncertainties.

Some interesting patterns can be seen in the $M1$ transitions. It is clear from Table III that the $B(M1)$ values for type A transitions (smaller energies) are consistently higher than those for type B decays. There are some suggestions from the branching and mixing ratios of increasing $M1$ strength in the vicinity of the proton crossing. However, it is not possible to draw any firm conclusions due to the limited lifetime data.

In order to interpret the effect on the $B(M1)$ values from the alignment of the $g_{9/2}$ proton pair one can employ the "semiclassical" model proposed in Ref. 7. The component of the magnetic moment which is perpendicular to the direction of the total angular momentum is composed of the neutron spin coupled to the symmetry axis and the spins of the two $g_{9/2}$ protons coupled to the axis of rotation. In the most recent formulation by Dönau[8] the $B(M1)$ rate is given by

$$B(M1, I\rightarrow I-1)=\frac{3}{8\pi}\left[\frac{K}{I}\right]^2\left\{(g_n-g_R)\left[(I^2-K^2)^{1/2}-i_n\pm\frac{I\Delta e'}{\omega}\right]-(g_p-g_R)i_p\right\}^2(\mu_N)^2\,, \tag{2}$$

where i_n and i_p are the spin alignment along the axis of rotation for the odd neutron and the $g_{9/2}$ protons, respectively. $\Delta e'$ is the signature splitting between the $\alpha=+\frac{1}{2}$ and $-\frac{1}{2}$ bands.

We have used the Schmidt values

$$g_j=g_l\pm(g_s-g_l)\left[\frac{1}{2l+1}\right],\quad j=\pm\tfrac{1}{2} \tag{3}$$

with $g_s=0.65g_{s,\text{free}}$ and $g=g_{\text{free}}$, which yield $g_n=-0.28$ and $g_p=1.29$. With $g_R=Z/A$, Eq. (2) gives for $J\approx 11/2$ (type B), $B(M1)\approx 0.02\ (\mu_N)^2$ and for $J\approx\frac{13}{2}$ (type A), $B(M1)\approx 0.54\ (\mu_N)^2$. After the proton crossing, Eq. (2) gives for $J\approx\frac{23}{2}$ (type B), $B(M1)\approx 0.55\ (\mu_N)^2$ and $\Delta J\approx\frac{25}{2}$ (type A), $B(M1)\approx 0.82\ (\mu_N)^2$. These results qualitatively reproduce the observed differences between type A and type B $M1$ strengths at lower spins. They are also in agreement with the possible increase in

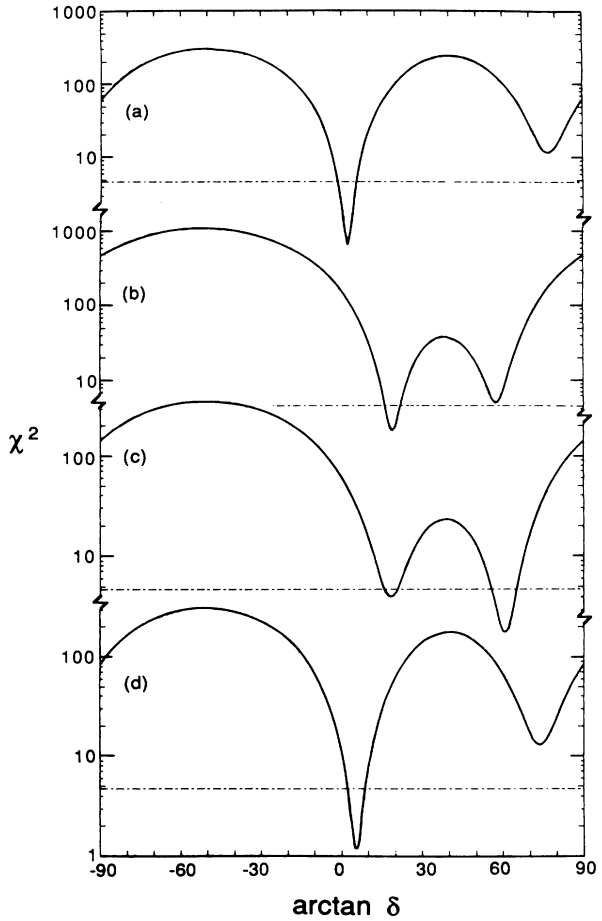

FIG. 6. Several χ^2 vs arctanδ plots are shown. The minima indicate the choice of δ, which is the mixing ratio $E2/M1$. (a), (b), (c) and (d) are the plots for the 218 keV, $\frac{13}{2}^+ \rightarrow \frac{11}{2}^+$; 506 keV, $\frac{11}{2}^+ \rightarrow \frac{9}{2}^+$; 790 keV, $\frac{19}{2}^+ \rightarrow \frac{17}{2}^+$; and 661 keV, $\frac{27}{2}^+ \rightarrow \frac{25}{2}^+$ transitions, respectively. The dashed line indicates the 0.1% confidence limit.

$B(M1)$ values after the proton alignment, especially for type B transitions. Such an increase has been seen[9] in ^{81}Kr.

V. INTERPRETATION

^{77}Kr lies the region of transitional neutron deficient nuclei around $Z=36$ and $N=40$, where strong variations in collective properties have been observed as functions of both neutron and proton number. In fact, nuclei with $Z=37$ [^{77}Rb (Ref. 10)] or $Z=38$ [^{78}Sr (Ref. 11)] are among the best collective rotors known. Quadrupole moments of these nuclei, of the order of $Q_0=3.3$ e b, suggest that they have very elongated shapes with a quadrupole deformation[12] $\beta_2=0.38$. On the other hand, nuclei with $Z<34$ are much less deformed and, in many of them, deformed prolate structures coexist with weakly deformed oblate bands. Neutron deficient Kr isotopes ($Z=36$) lie just in the center of the region: At low spins the shape coexistence pattern is clearly seen, but at higher angular momenta they behave fairly collectively. All these variations can be well explained by means of the deformed shell model, where observed properties can be directly associated with the large prolate and oblate energy gaps in the single-particle spectrum.[12,13]

Both even-even cores of ^{77}Kr, i.e., ^{76}Kr and ^{78}Kr, are predicted to be prolate deformed in their ground states but γ soft. Calculations of Ref. 12 based on the shell correction method with the deformed Woods-Saxon average field predict a 0.55 MeV energy difference between coexisting prolate ($\beta_2=0.35$) and oblate ($\beta_2=-0.31$) minima in ^{76}Kr and almost no difference in energy between the prolate ($\beta_2=0.30$) and oblate ($\beta_2=-0.25$) configurations in ^{78}Kr. These predictions are well correlated with the observed excited weakly deformed structure in ^{76}Kr (Ref. 11) and with a decrease in the observed quadrupole moments and moments of inertia[1,3,14,15] when going from ^{76}Kr to ^{78}Kr. Because both ^{77}Kr cores are β and γ soft, one may expect shape polarization effects due to rotationally aligned quasiparticles to be seen in this nucleus. Such effects have recently been reported in the odd-proton nucleus ^{75}Br (Ref. 4).

A. Experimental quasiparticle energies and alignments

In order to discuss rotational properties of the observed bands in ^{77}Kr, we performed a cranked shell model[16] analysis of the experimental data. Figure 7 shows quasiparticle Routhians e' and aligned angular momenta i for the positive parity yrast bands in ^{77}Kr compared to the ground-state rotational bands in ^{76}Kr (Ref. 17) and ^{78}Kr (Ref. 3). Because of the band mixing effects and shape variations due to the centrifugal stretching at low spins, the choice of reference parameters J_0 and J_1 causes some problems. To fix a reference curve we thus used the three-quasiparticle unfavored $\pi=+$ band ($I>\frac{27}{2}$) in ^{77}Kr which has a fairly constant moment of inertia.

Both positive parity bands in ^{77}Kr are built on the $\nu g_{9/2}$ intruder orbital [422 $\frac{5}{2}$]. Because of the blocking argument the first crossing in these bands must be due to the alignment of the $g_{9/2}$ proton pair. Such strong crossing with a small interaction matrix element has indeed been observed at $\hbar\omega=0.51$ MeV in the unfavored ($\alpha=-\frac{1}{2}$) band. The favored band ($\alpha=+\frac{1}{2}$) undergoes a gradual alignment in the frequency interval $0.53<\hbar\omega<0.64$ MeV which can be associated with a large band interaction. The gain in alignment in both bands is about 4.5 $\hbar$ which nicely agrees with the aligned angular momenta in the 1qp proton bands in ^{75}Br: $i(\alpha=\frac{1}{2})=2.8$ $\hbar$ and $i(\alpha=-\frac{1}{2})=1.5$ $\hbar$ (Ref. 4). At higher frequencies, $\hbar\omega>0.75$ MeV, a further increase in alignment begins. We will argue in Sec. V C that this can be associated with the alignment of the $g_{9/2}$ neutron pair.

By subtracting the contribution from the ^{76}Kr core one obtains $i(\alpha=\frac{1}{2})=1.8$ $\hbar$ and $i(\alpha=-\frac{1}{2})=1$ $\hbar$ for the aligned angular momenta in the 1qp $\nu g_{9/2}$ states in ^{77}Kr. By summing up the contributions from protons (4.5 $\hbar$) and neutrons (2.8 $\hbar$) one obtains $i=7.3$ $\hbar$—the gain in

TABLE III. Transition strengths in ^{77}Kr.

J^π	E_γ (keV)	Type	τ (ps)[a]	$\Delta J=2$ $B(E^2)$ (e^2 fm^4)	$\Delta J=1$ $B(E2)$ (e^2 fm^4)	$\Delta J=1$ $B(M1)$ (μ_N^2)[b]
$\frac{11}{2}^+$	506	*B*	3.0(5)		672^{+341}_{-303}	$0.098^{+0.026}_{-0.020}$
	634			664^{+213}_{-174}		
$\frac{13}{2}^+$	218	*A*	2.7(3)		99^{+344}_{-99}	0.37±0.08
	724			1247^{+186}_{-155}		
$\frac{15}{2}^+$	657	*B*	1.2(2)		113^{+74}_{-68}	$0.077^{+0.022}_{-0.018}$
	874			694^{+192}_{-152}		
$\frac{17}{2}^+$	258	*A*	0.90(15)		255^{+450}_{-255}	0.15±0.06
	915			1358^{+286}_{-208}		
$\frac{19}{2}^+$	790	*B*	0.4(2)		228^{+263}_{-111}	$0.097^{+0.016}_{-0.041}$
	1048			1018^{+1065}_{-388}		
$\frac{21}{2}^+$	282	*A*	0.26(8)[c]			0.59–0.50[d]
	1072			>2019		
$\frac{23}{2}^+$	781	*B*	0.3–4[e]		(366–252)	(0.23–0.17)
	1063			(782–587)		
$\frac{25}{2}^+$	382	*A*	0.44(15)[c]		178^{+447}_{-178}	$0.37^{+0.24}_{-0.14}$
	1163			733^{+396}_{-203}		

[a]Reference 1.
[b]Nuclear magneton $\mu_N = e\hbar/2M_p c$.
[c]Lifetimes not corrected for side feeding.
[d]Value for $0 \leq |\delta| \leq 0.4$ and a branching ratio of 6%.
[e]Estimated typical lifetime range.

alignment for the even-even system after proton and neutron crossings. One can see in Fig. 7 that this is precisely the value for the gain in angular momentum in ^{76}Kr in the region of rotational frequency between $0.55 \leq \hbar\omega \leq 0.75$ MeV. On the basis of this simple additivity argument, one may draw the conclusion that the backbending observed in ^{76}Kr results from the consecutive alignment of the $g_{9/2}$ proton and $g_{9/2}$ neutron pairs. It has been shown in Ref. 4 that in ^{76}Kr the expected proton crossing frequency is slightly lower ($\hbar\omega=0.6$ MeV) than the neutron one ($\hbar\omega=0.68$ MeV) at the deformation appropriate for this nucleus. This result can easily be understood: In the Kr isotopes with $N>40$ the proton Fermi surface penetrates the first half of the $g_{9/2}$ shell, while the neutron Fermi surface lies in the region of deformation-aligned states above the [422 $\frac{5}{2}$] orbital. Therefore the $g_{9/2}$ proton pair carries more aligned angular momentum than does the pair of decoupled $g_{9/2}$ neutrons and, consequently, protons are expected to align first. With increasing neutron number the difference between the proton and neutron crossing frequencies should be even larger. In ^{78}Kr the first crossing occurs at $\hbar\omega=0.56$ MeV and the corresponding gain in alignment is 4.5–5 $\hbar$ (cf. Fig. 7)—characteristic of the alignment of the $g_{9/2}$ proton pair. So far no neutron crossing has been observed in this nucleus.

The signature splitting between $\pi=+$ Routhians in ^{77}Kr increases with rotational frequency, reaching the value of 250 keV at $\hbar\omega=0.5$ MeV. After alignment of the proton pair the signature splitting is reduced to the value of 100 keV at $\hbar\omega=0.65$ MeV. Such variation in the signature splitting is not expected for a system with rigid deformation and indicates the shape change associated with the quasiparticle alignment (cf. Sec. V C below).

In order to explain alignment properties and shape variations in ^{77}Kr, deformation–self-consistent cranking calculations were carried out. They are described in the following sections.

B. Remarks about the model

If the core of the nucleus is deformation-soft, rotationally aligned quasiparticles will have a large influence on the overall nuclear shape.[18] Experimental data discussed in the previous section—the shifts in the frequency of the first proton crossing and changes in the signature splitting—suggest that this is exactly the case in ^{77}Kr. In order to investigate the influence of shape effects on the rotational properties of ^{77}Kr we have performed

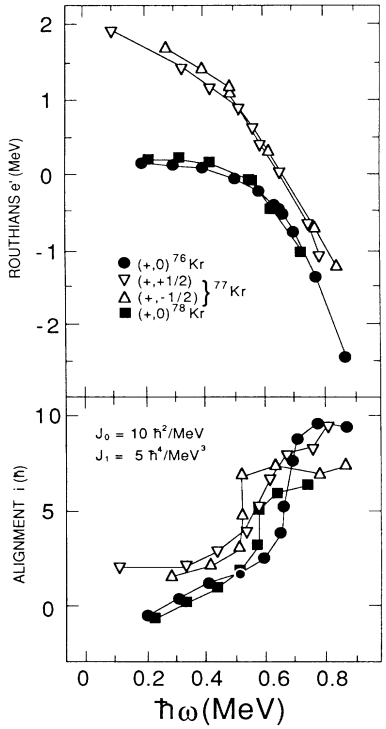

FIG. 7. Experimental intrinsic frame excitation energies (Routhians) and alignments for $^{76-78}$Kr as a function of the rotational frequency $\hbar\omega$. Experimental data for ^{76}Kr and ^{78}Kr were taken from Refs. 17 and 3, respectively.

Strutinsky-Bogolyubov cranking calculations using the nonaxial Woods-Saxon potential[12,19] with the parameters of Ref. 20. The pairing interaction was assumed to be of the monopole-pairing type with state-independent pairing strengths G_n and G_p for neutrons and protons. They were taken according to Ref. 12. Rotation was taken into account using the usual cranking ansatz:

$$H' = H - \omega I_x \ , \tag{4}$$

where I_x is the projection of the angular momentum operator onto the cranking axis.

At zero rotational frequency the pairing gap, Δ(BCS), was calculated using the BCS method. At high spins the Coriolis force acts destructively on the mean pair field with a corresponding reduction of the static gap parameter. Within the Hartree-Fock Bogolyubov cranking approximation the pairing gap suddenly drops to zero at a critical value of rotational frequency,[21] $\omega_{\rm crit}$. In the $A=80$ nuclei this pairing phase transition would occur roughly at $\hbar\omega_{\rm crit}=0.7$ MeV, in conjunction with the alignment of one pair of quasiparticles. Within the particle-number conserving approaches, however, the pairing correlations are present to some extent at all frequencies. Having this in mind, we approximate the average pairing properties at high spins by parametrizing the pairing gap as a smooth function of ω:

$$\Delta(\omega) = \begin{cases} \Delta(\mathrm{BCS}) \left[1 - \frac{1}{2} \left[\frac{\omega}{\omega_{(\rm crit)}} \right]^2 \right], & \omega < \omega_{(\rm crit)} \\ \Delta(\mathrm{BCS}) \left[\frac{1}{2} \left[\frac{\omega_{(\rm crit)}}{\omega} \right] \right], & \omega > \omega_{(\rm crit)} \ , \end{cases} \tag{5}$$

with $\omega_{\rm crit}=0.7$ MeV for both neutrons and protons.

The nuclear shape was defined by the standard (β_2,γ) parametrization. Hexadecapole deformation, β_4, was included in a similar way as in Ref. 12. Three (β_2,γ) planes of dimension 9×8 (cf. Ref. 12) corresponding to three different values of β_4 have defined our deformation space $(\tilde{\beta})$.

The total Routhian of a nucleus (Z,N) of fixed many-quasiparticle configuration ν is given by

$$E'_\nu(N,Z,\tilde{\beta},\omega) = E_{\rm Strut}(N,Z,\tilde{\beta}) + [\langle \psi_\nu | H^\omega | \psi_\nu \rangle - \langle \psi_\nu | H^\omega | \psi_\nu \rangle |_{\omega=0}] \ , \tag{6}$$

where $E_{\rm Strut}(N,Z,\tilde{\beta})$ is the energy of the nonrotating state obtained by the Strutinsky method[22] and the term in square brackets represents the rotational energy in the intrinsic system of coordinates. At a fixed value of rotational frequency the total routhian [Eq. (6)] was minimized with respect to the shape parameters $\tilde{\beta}$ by interpolating between the lattice points.

A detailed description of these calculations will be published in a separate paper.[23]

C. Shape changes and alignment properties

In Ref. 12 the low-lying bandheads of ^{77}Kr were calculated. On the prolate side the two lowest single-particle states, $[422\,\frac{5}{2}]$ and $[301\,\frac{3}{2}]$ were associated with the quadrupole deformation $\beta_2=0.33$. In addition, calculations indicate the presence of excited oblate structures originating from the $g_{9/2}$ and $p_{1/2}$ orbitals with quadrupole deformations ranging between -0.22 and -0.26.

Results of our calculations for ^{77}Kr are summarized in Fig. 8 where equilibrium deformations for the lowest quasiparticle configurations of different parity π and signature α are displayed for a sequence of rotational frequencies as explained in the figure caption

1. *The $g_{9/2}$ prolate bands*

At low spins the $g_{9/2}$ prolate bands correspond to a shape with quadrupole deformation around $\beta_2=0.34$ and negative γ deformation decreasing from $\gamma=-2°$ to $-8°$ due to the centrifugal stretching. The appropriate quasiparticle diagram is shown in Fig. 9. At $\hbar\omega=0.5$ MeV a first band crossing, corresponding to an alignment of a pair of $g_{9/2}$ protons, appears. Two aligned quasiprotons drive the deformation towards smaller values of β_2 and positive γ values ($\gamma=10°$). At this shape the signature splitting between the $g_{9/2}$ Routhians is reduced (see Fig. 10) which nicely explains experimental findings. Alignments of the $g_{9/2}$ neutron pairs (AD and BC crossings)

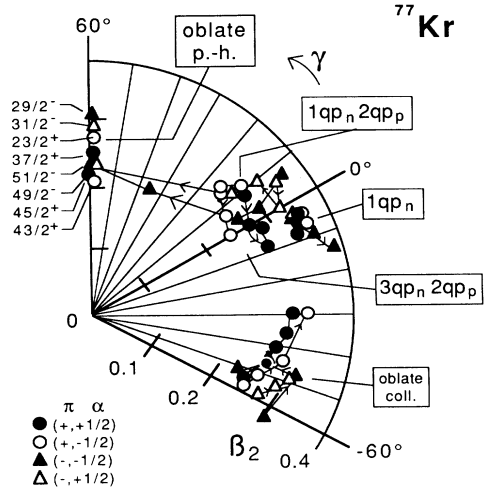

FIG. 8. Calculated equilibrium deformations (β_2,γ) for the lowest quasiparticle configurations in ^{77}Kr. The total Routhian (Ref. 2) [Eq. (6)] has been minimized at each (β_2,γ) grid point with respect to β_4. Small arrows indicate the direction of increasing rotational frequency (in the present diagram $\hbar\omega$ was varied in the interval $0<\hbar\omega<1$ MeV). Labels indicate characteristic quasiparticle structures. Note the dramatic shape changes associated with increasing the number of aligned quasiparticles.

are predicted to occur at $\hbar\omega=0.66$ MeV, slightly below the experimental value. It is seen in Fig. 10 that the band interaction in the favored band (*BC* crossing) is much smaller than that in the unfavored band (*AD* crossing), which is consistent with the results shown in Fig. 7. Since the neutron Fermi surface lies in the upper part of the $g_{9/2}$ shell, the aligned $g_{9/2}$ neutrons trigger a change to more negative γ values ($\gamma\approx 0°$) (see Ref. 13).

2. *The $\pi=-$ prolate bands*

The low spin behavior of $\pi=-$ bands is very similar to that predicted for the $g_{9/2}$ structures. As the neutron $g_{9/2}$ orbitals are not blocked in these bands, one should

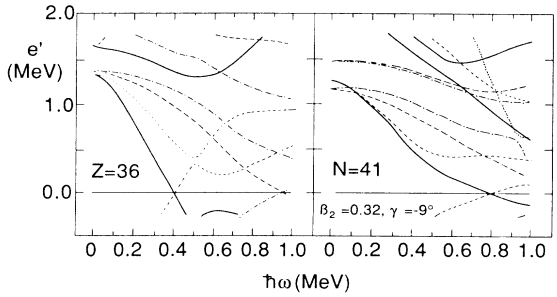

FIG. 9. Proton and neutron quasiparticle Routhians in ^{77}Kr at deformation $\beta_2=0.32$, $\gamma=-9°$ representative for the 1qp$_{(\nu)}$ configurations in Fig. 10. Routhians are labeled by means of parity π and signature α quantum numbers: solid line ($\pi=+$, $\alpha=\frac{1}{2}$), short-dashed line ($\pi=+$, $\alpha=-\frac{1}{2}$), long-dashed line ($\pi=-$, $\alpha=\frac{1}{2}$), and dash-dotted line ($\pi=-$, $\alpha=-\frac{1}{2}$).

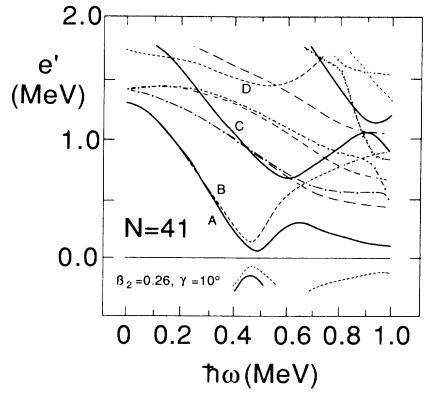

FIG. 10. Same as in Fig. 9 but for neutrons at deformation $\beta_2=0.26$, $\gamma=10°$, representative for the 1qp$_{(\nu)}$2qp$_{(\pi)}$ configurations of Fig. 10.

expect the neutron alignment to follow the proton crossing, as in the case of ^{76}Kr. Reduction in the γ deformation when going from the 3qp to the 5qp $\pi=-$ band seen in Fig. 8 reflects this double crossing. At a higher rotational frequency both negative parity bands terminate at the oblate axis at the optimal particle-hole states $J^\pi=\frac{51}{2}^-$ and $\frac{49}{2}^-$.

3. *The noncollective oblate states*

A few low-lying particle-hole configurations have been predicted to appear low in energy. Their deformations vary between $\beta_2=0.2$ and 0.3 ($\gamma=60°$) (see Fig. 8). The most favored ones predicted by the calculations are

$$J^\pi=\tfrac{32}{2}^+=\nu[(g_{9/2})^3_{21/2}(p_{3/2})^4_0]\pi(g_{9/2})^2_8\ ,$$

$$J^\pi=\tfrac{51}{2}^-=\nu[(g_{9/2})^4_{12}(p_{3/2})^3_{3/2}]\times\pi[(g_{9/2})^2_8(p_{3/2})^1_{3/2}(f_{5/2})^1_{5/2}]\ .$$

So far no such noncollective states have been seen experimentally.

4. *Collective oblate states*

At the oblate shape ($\gamma=-60°$) a few rotational bands are predicted to lie low in energy. At low spins they can be interpreted as 1qp excitations coupled to the excited oblate minimum in ^{76}Kr. In our calculations these collective oblate states appear higher in energy than the near-prolate bands and they never become yrast. The calculations predict an increase in the γ deformation for these bands, both due to centrifugal stretching and quasiparticle alignment.

VI. CONCLUSIONS

The yrast band in ^{77}Kr has been extended up to spin $J^\pi=(\frac{41}{2}^+)$. The strong signature splitting seen below $J^\pi=\frac{25}{2}^+$ is weaker after two $g_{9/2}$ protons align, indicating a shape change toward smaller β_2 and positive γ values. The amount of alignment gained from the neutrons in ^{77}Kr and the protons in ^{75}Br compare nicely

with the alignment gain seen in ^{76}Kr. Above the $J^{\pi}=\frac{33}{2}^{+}$ state the signature splitting strengthens, suggesting the alignment of a pair of neutrons. The $\Delta J=1$ transitions are not visible, perhaps indicating that the aligning neutrons reduce the total magnetic moment.

Angular distribution results indicate mixed $E2/M1$ transitions alternating with almost pure $M1$ transitions in the 1qp band. The $B(M1)$ transition rates also alternate in strength in qualitative agreement with a simple model[8] proposed by Dönau. After the proton crossing these $\Delta J=1$ transitions have almost pure $M1$ character.

The observed structure of ^{77}Kr compares well with what has been seen in the neighboring nuclei. There are indications (mixing and branching ratios) that ^{77}Kr may be an intermediate case of the phenomenon seen in ^{81}Kr, where strong $\Delta J=1$ transitions dominate the 3qp band. Thus, further theoretical work and experimental lifetime measurements examining these $M1$ transitions may prove fruitful.

ACKNOWLEDGMENTS

This work was supported in part by the National Science Foundation, the Danish Natural Science Research Council, and the Florida State University Supercomputer Computations Research Institute, which is partially funded by the U.S. Department of Energy through Contract No. DE-FC05-85ER250000.

*Present address: Chemistry Department, Eastern Mennonite College, Harrisonburg, VA 22801.

†On leave of absence from Institute of Physics, Warsaw Institute of Technology, PL-00662 Warsaw, Poland.

[1]B. Wörman, K. P. Lieb, R. Diller, L. Lühmann, J. Keinonen, L. Cleemann, and J. Eberth, Nucl. Phys. **A431**, 170 (1984).

[2]E. Nolte and P. Vogt, Z. Phys. A **275**, 33 (1975).

[3]H. P. Hellmeister, J. Keinonen, K. P. Lieb, U. Kaup, R. Rascher, R. Ballini, J. Delaunay, and H. Dumont, Nucl. Phys. **A332**, 241 (1979).

[4]L. Lühmann, M. Debray, K. P. Lieb, W. Nazerewicz, B. Wörmann, J. Eberth, and T. Heck, Phys. Rev. C **31**, 828 (1985).

[5]M. E. Rose and D. M. Brink, Rev. Mod. Phys. **39**, 306 (1967).

[6]P. Taras and B. Haas, Nucl. Instrum. Methods **123**, 73 (1975).

[7]F. Dönau and D. S. Frauendorf, in *High Angular Momentum Properties in Nuclei,* edited by N. R. Johnson (Harwood Academic, Chur, Switzerland, 1983), p. 143.

[8]F. Dönau, Niels Bohr Institute report, 1985.

[9]L. Funke, J. Döring, P. Kemnitz, E. Will, G. Winter, A. Johnson, L. Hildingsson, and Th. Lindblad, Nucl. Phys. **A455**, 206 (1986).

[10]L. Lühmann, K. P. Lieb, C. J. Lister, J. W. Olness, H. G. Price, and B. J. Varley, Europhys. Lett. **1**, 623 (1986).

[11]C. J. Lister, B. J. Varley, H. G. Price, and J. W. Olness, Phys. Rev. Lett. **49**, 308 (1982).

[12]W. Nazarewicz, J. Dudek, R. Bengtsson, T. Bengtsson, and I. Ragnarsson, Nucl. Phys. **A435**, 397 (1985).

[13]R. Bengtsson and W. Nazarewicz, in Proceedings of the XIXth Winter School on Physics, Zakopane, 1984, edited by Z. Stachura, p. 171.

[14]R. B. Piercey, A. V. Ramayya, J. H. Hamilton, X. J. Sun, R. L. Robinson, H. J. Kim, and J. C. Wells, Phys. Rev. C **25**, 1941 (1982).

[15]R. L. Robinson, H. J. Kim, R. O. Sayer, W. T. Milner, R. B. Piercey, J. H. Hamilton, A. V. Ramayya, J.C. Wells, Jr., and A. J. Caffrey, Phys. Rev. C **21**, 603 (1980).

[16]R. Bengtsson and S. Frauendorf, Nucl. Phys. **A327**, 139 (1979); **A314**, 27 (1979).

[17]K. P. Lieb, in *Proceedings of the International Symposium on Weak and Electromagnetic Interactions in Nuclei,* Heidelberg, 1986, edited by H. V. Klapdor (Springer-Verlag, Berlin, 1986), p. 106.

[18]S. Frauendorf and F. R. May, Phys. Lett. **152B**, 245 (1983).

[19]S. Ćwiok, J. Dudek, and W. Nazarewicz (unpublished).

[20]J. Dudek, Z. Szymański, and T. Werner, Phys. Rev. C **23**, 920 (1981).

[21]B. R. Mottelson and J. G. Valatin, Phys. Rev. Lett. **5**, 511 (1968).

[22]V. M. Strutinsky, Nucl. Phys. **A95**, 420 (1967).

[23]W. Nazarewicz, G. A. Leander, and S. L. Tabor (unpublished).